JOURNAL OF Materials CHEMISTRY

Fluorescence and physical characterization of sol–gel-derived nanocomposite films suitable for the entrapment of biomolecules†

Gillian L. G. Goring and John D. Brennan*

Department of Chemistry, McMaster University, Hamilton, Ontario, Canada L8S 4M1. E-mail: brennanj@mcmaster.ca

Received 10th May 2002, Accepted 16th August 2002
First published as an Advance Article on the web 13th September 2002

Thin films (100–500 nm thick) of Class I, Class II and Class I/II organic–inorganic hybrid silicates were prepared by casting mixtures of tetraethyl orthosilicate, methyltriethoxysilane and/or dimethyldimethoxysilane that were first hydrolyzed *via* sonication using acid catalysis, followed by induction of gelation using added buffer solutions containing no polymer or 3% w/v of poly(ethylene glycol). In some cases, the fluorescent probe 6-propionyl-2-dimethylaminonaphthalene (PRODAN) or the protein human serum albumin (HSA) were also added to the buffer solution, which permitted the fluorescence probing of the internal environment and biological activity within the various silicate films, respectively. Parameters such as the type and level of organosilane precursor, polymer level, casting speed, and aging time were varied to determine how such factors affected the thickness, morphology, and internal environment of the resulting films that were formed by this two-step process. The results show that composite films evolve in two stages: (1) rapid drying during the initial 1–2 h after casting of the film, followed by (2) a slower aging process that continues for many months. The aging of these thin films is different to that of bulk materials and the final state of the films can be quite different from that obtained for bulk materials. Preliminary studies of HSA-doped films show that the entrapped protein adopts a partially expanded conformation, but in most cases is still able to bind to ligands.

Introduction

The sol–gel process offers a promising route for the development of nanocomposite materials.[1–6] Hydrolysis and condensation of tetraalkoxysilanes can be done in the presence of either a dispersed additive such as an organic polymer, producing a Class I material,[7–11] or along with an organosilane, leading to Class II materials with covalently anchored functional groups.[7,10,12,13] Incorporation of both dispersed and anchored organic groups is also possible, leading to Class I/II nanocomposite materials.

An emerging area that is attracting increased attention is the development of biologically-doped nanocomposite materials, which are useful for the development of biosensing devices. Encapsulation of biologicals *via* the sol–gel process typically involves the hydrolysis of an alkoxysilane precursor in the absence of added alcohol, followed by addition of a buffered solution containing the protein of interest to promote gelation. The addition of buffer brings the pH to the physiological range of 7.5 $\pm$ 1.0 and dilutes the alcohol produced during hydrolysis. Low temperature aging over a period of several weeks or months results in a durable, optically clear biomaterial which shows good retention of protein activity, as summarized by Avnir *et al.*[14]

Most research describing biologically-doped sol–gel materials has focused on the preparation of bulk glasses (*i.e.* glass blocks or slides) with thicknesses of the order of several hundred micrometers up to 1 cm.[15,16] Bulk glasses allow sufficient amounts of the biomolecule to be entrapped to permit spectroscopic or electrochemical investigations, but suffer from drawbacks such as long aging times and extremely slow response times.[10] Therefore, it is generally agreed that thin films (*i.e.* submicron thickness) are most appropriate for the development of analytical devices, such as biosensors. Thin films age rapidly, thereby limiting drifts in calibration,[17] offer fast response times[18] and can be interfaced to planar waveguide or standard fiber optic-based biosensors to allow internal reflection fluorescence measurements.[19,20]

Sol–gel-derived thin films can be prepared by a variety of methods, including spin casting,[21,22] dip casting,[16,17,23,24] and aerosol spraying.[5,22,25] While such films have been successfully utilized for chemical or biosensor development, numerous drawbacks remain to be overcome. First, many of the film formation protocols (*i.e.* spin casting, aerosol deposition) are not amenable to coating the curved surface of substrates such as optical fibers, which may limit their utility for remote sensing.[26,27] Second, thin films generally require high levels of the biomolecule for sufficient signal to be generated, making it problematic for species such as proteins that are insoluble and/or aggregate in the alkoxysilane solution.[18] Third, high levels of alcohol are often required as a viscosity modifier to allow proper formation of a dip-cast thin film,[28] leading to denaturation of the encapsulated biomolecules.[21] Finally, thin films undergo substantial changes in structure and solvent content on a short timescale during the aging and drying process,[28] potentially leading to extensive cracking[29,30] and dehydration of encapsulated biologicals.[5,31,32]

The primary objective of this work is to prepare and characterize sol–gel-derived thin films formed *via* the dip casting method that cover the range of undoped, Class I, Class II, and Class I/II organic–inorganic nanocomposites. A multi-step processing protocol is described that begins with the sonication of mixtures of tetraethyl orthosilicate (TEOS) and an organosilane precursor in the absence of added alcohol to promote hydrolysis. A carefully chosen buffer (containing a fluorescent dye, polymer, and/or protein) is then mixed with the hydrolyzed silane to promote a slow gelation process that occurs over a period of an hour or more. A substrate is cast into the silane mixture to transfer a small volume of the silane onto its surface, resulting in a thin film containing the entrapped dye, polymer, and/or protein.

The physical characteristics of these composite films have

†Electronic supplementary information (ESI) available: table of gelation times of silane mixtures used to produce thin films. See http://www.rsc.org/suppdata/jm/b2/b204547h/

 DOI: 10.1039/b204547h

been characterized using profilometry and optical microscopy to yield information on film thickness, morphology, cracking, and durability. These results and are compared to previous results obtained from both monoliths and thin films that are formed without the addition of buffered aqueous solutions. The internal environment of the films, and their evolution over time, has also been examined by entrapping the dipolarity-sensitive fluorescent probe 6-propionyl-2-dimethylamino-naphthalene (PRODAN)[33] into the films. This probe has been used previously to investigate the internal environment of sol–gel-derived monoliths, and thus allows for comparison of the internal environment and drying times between monoliths and thin films.[34] Studies of films containing human serum albumin (HSA) are also presented, showing that HSA remains functional and accessible to ligands when entrapped in such films. The results show that films produced using the two-step preparation method are amenable to the entrapment of biomolecules, can be tuned to optimize protein stability, and thus should be useful for the development of bioanalytical devices.

Experimental

Chemicals

Poly(ethylene glycol) (PEG, MW 600), tetraethyl orthosilicate (TEOS, 99.999+%), methyltriethoxysilane (MTES, 98%), and dimethyldimethoxysilane (DMDMS, 98%) were purchased from Aldrich (Milwaukee, WI, USA) and were used without further purification. Human serum albumin (HSA, essentially fatty acid free), salicylic acid, and polymethacrylate fluorimeter cuvettes (transmittance curve C) were obtained from Sigma (St. Louis, MO, USA). Guanidine hydrochloride (GdHCl, Sequanol grade) was obtained from Pierce (Rockford, IL, USA). Sephadex G-75 fine powder was supplied by Pharmacia Biotech (Uppsala, Sweden). 6-propionyl-2-dimethylamino-naphthalene (PRODAN) was obtained from Molecular Probes (Eugene, OR, USA). Glass microscope slides, which were used for casting of thin films, were obtained from Fisher Scientific (Toronto, ON, Canada). Quartz microscope slides (for HSA studies) were obtained from Chemglass (Vineland, NJ, USA). All slides were cut to approximate dimensions of 8 × 32 mm. All water was purified by reverse osmosis and deionized using a Milli-Q Synthesis A10 4-stage water purification system. All other chemicals and solvents used were of analytical grade and were used without further purification.

Procedures

Cleaning of substrates. A variety of methods were investigated for cleaning of glass and quartz slides to maximize the adhesion of sol–gel-derived thin films. The best method was found to be one that involved soaking the slides in 1.0 N NaOH for 18–24 h, followed by rinsing with water and methanol. The substrates were then dried at room temperature under a stream of nitrogen. Clean slides generally showed contact angles for water droplets close to 0°, indicative of a hydrophilic surface. Clean slides were typically stored in a dust-free container and used within 1 day of cleaning to avoid contamination.

Preparation of sol–gel-derived thin films. Precursor solutions contained either 100% TEOS or molar ratios of 20% MTES : TEOS or 10% DMDMS : TEOS. 4.5 mL of the silane mixture was combined with 1.4 mL of water and 0.1 mL of 0.1 N HCl and sonicated until the mixture was visibly homogeneous. The silane solutions were used immediately for preparation of thin films.

0.5 mL of the appropriate silane solution was thoroughly mixed with an equivalent volume of buffer solution (10 to 100 mM Tris at pH 7.2) containing 100 mM KCl, 0–10% (w/v) of PEG, and either 4.5 μM of PRODAN or 35 μM of HSA, and the mixture was transferred to a Teflon casting well. A clean glass slide mounted on a motorized dip caster (Kibron Layer-X filmlift, Helsinki, Finland) with a vertically moving arm was cast into the solution at 10 mm min^{-1} and then withdrawn at rates varying from 1 to 10 mm min^{-1}. The cast films were either tested immediately or suspended in air at room temperature for 10 min, and then placed into a disposable cuvette that was sealed with Parafilm and stored in the dark for 72 h at 4 °C before testing, unless otherwise stated.

Fluorescence spectroscopy. Fluorescence spectra were collected using instrumentation and procedures described elsewhere.[35] Emission spectra for samples containing PRODAN were collected using slides suspended in air at a temperature of 20 ± 0.2 °C. The glass slides were mounted at an angle of 55° with respect to the excitation beam, such that the excitation radiation was reflected away from the emission PMT. Samples containing HSA were excited at 295 nm, while those containing PRODAN were excited at 370 nm, with emission collected over the entire emission band in each case. Appropriate blanks were subtracted from each sample and the spectra were corrected for deviations in emission monochromator throughput and PMT response.

Profilometry. All profilometry measurements were performed using a Tencor Instruments (Mountain View, CA, USA) Alpha-Step 100 profilometer. The stylus was positioned over the uncoated portion of the slide in order to obtain a baseline height measurement. The stylus was moved from the uncoated region to the coated region of the slide at a rate of 6 mm min^{-1} and the film height difference was continuously monitored using a strip-chart recorder with a scale of 25 000 Å cm^{-1}. The results reported are the average of at least three regions per film for a minimum of three different films. Optical micrographs were acquired subsequent to profilometry to ensure that the tip did not penetrate the surface.

Optical microscopy. Micrographs were obtained using an Olympus microscope with a CCD video camera and a 10× objective. Images were obtained from films immediately after casting, after 24 h, and after 21 days of aging. In each case, images were obtained both before and after the rehydration of the film, which was accomplished by submerging the film in water for 10 min. The image area in all cases is 1.1 mm × 0.8 mm (magnification factor is 400×).

Salicylate titrations of HSA. Slides coated with HSA-doped films were placed into polymethacrylate fluorimeter cuvettes containing 2.0 mL of a 10 mM Tris buffer. The samples were titrated with 100 μM salicylate in 10 mM phosphate buffer at pH 7.2. Fluorescence emission spectra were collected at various levels of salicylate to monitor the quenching of Trp-214 by salicylate. The spectra were corrected for blank contributions using a solution containing salicylate but no protein, and a 10 nm window centered at 335 nm was integrated to provide intensity values for the protein at each salicylate concentration.

Results and discussion

Physical characteristics of thin films

Preparation of thin films. The main factors that are important in development of thin biofilms are the thickness of the film, its adhesion to the substrate, its resistance to cracking, the internal microenvironment, and the potential for leaching of entrapped species. Factors that were optimized to achieve useful films included substrate surface treatment prior to casting, buffer type and concentration (to control gelation times), silane type and content (to control film dipolarity), the

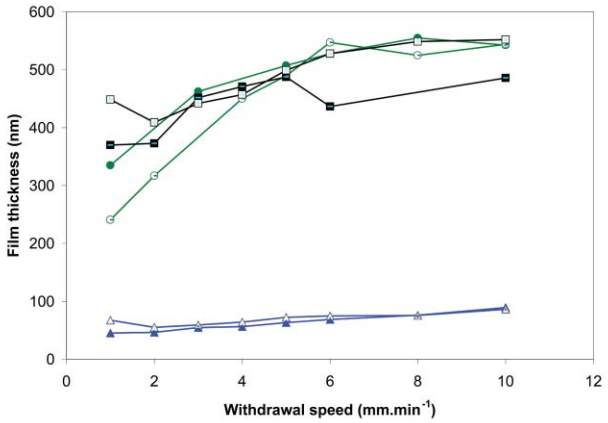

Fig. 1 Thickness values obtained for films composed of TEOS (■), TEOS + 3% PEG (□), 20% MTES (●), 20% MTES + 3% PEG (○), 10% DMDMS (▲), 10% DMDMS + 3% PEG (△) as a function of withdrawal speed. Typical errors are ± 30 nm.

presence of polymer additives, and the substrate withdrawal speed. These parameters were found to have significant effects on film thickness, clarity, cracking, and internal dipolarity, as described in detail below.

The adhesion of the film depended on both the method used to clean the substrate, and on the film thickness. Substrates that were cleaned using concentrated or dilute HF or H_2SO_4 did not provide good film adhesion, and introduced unwanted hazards related to handling of these materials. On the other hand, soaking of substrates in 1 N NaOH for 24 h led to surfaces that provided good adhesion of thin films. It was also found that films greater than 1 μm thick did not adhere to any substrate, regardless of the cleaning procedure used, thus, submicron thicknesses were required to produce durable films.

The thickness of the sol–gel-derived films was highly dependent on the gelation behavior of the sol, as gelation time had a tremendous impact on the viscosity of the casting solution. The major factors affecting the rate of gelation of the hydrolyzed silane when mixed with the buffer solution were: (1) the ratio and type of organosilane present in the silane solution; (2) the concentration and molecular weight of the polymer additive; (3) the type and concentration of buffer used; (4) the buffer pH. The gelation time increased as the amount of organosilane or polymer increased, and also increased as the buffer pH was increased or as the buffer concentration was decreased (see Table S1 in ESI). The gelation time also increased on going from TEOS to MTES to DMDMS, suggesting that steric effects partially controlled the gelation rate, and gelation time decreased dramatically when phosphate buffer was used, owing to phosphate-based catalysis of gelation.[36] Based on the studies of the film properties, as presented below, it was determined that the optimal gelation time was in the range of 60 to 180 min. Samples with shorter gelation times were noticeably more viscous, even immediately after mixing, and produced thick films of poor quality which often peeled away from the substrate, making them unsuitable for protein entrapment. Accessing longer gelation times required low ionic strength and pH values that were not compatible with the retention of protein function. The method adopted for the formation of optimal thin films involved the addition of a buffer solution (10 mM TRIS buffer, pH 7.2 with 100 mM KCl) containing either 0 or 3% PEG (higher values led to viscous casting solutions, which produced thick films that cracked extensively) along with the desired probe or protein, to an equal volume of the hydrolyzed silane (containing 100% TEOS, 20% MTES, or 10% DMDMS).

Thickness and morphology. Fig. 1 shows the thickness values obtained for films composed of TEOS, 20% MTES, and 10% DMDMS, with and without 3% PEG, as a function of withdrawal speed. It must be noted that film thickness was dependent on the time elapsed between mixing the silane and the buffer and the casting of the film, with thicker films being formed as the time after mixing increased, owing to increased viscosity of the casting solution. Thus, all data is reported for films that were cast immediately after mixing of the hydrolyzed silane and buffer. As shown in Fig. 1, film thickness increased with increased casting rates, as a result of increased drainage of the deposited solution.[15] Inclusion of PEG 600 at a level of 3% or less did not produce significant changes in thickness, indicating that such levels of the polymer do not alter the ability to cast thin films. Inclusion of PEG at higher levels led to much thicker films (>1 μm, data not shown) owing to the increased viscosity of the polymer-doped solutions.[15] Thickness was also dependent on the type of organosilanes present, increasing in the order DMDMS < MTES ≈ TEOS, owing to lower levels of cross-linking and correspondingly lower viscosities for the organosilane-doped films, which is consistent with the longer gelation times for such species.

Fig. 2 shows optical micrographs of the six different types of films obtained at a withdrawal speed of 4 mm min^{-1} (images a–f) along with two images of films after the addition of water (images g and h). All images show the middle region of the film, and reveal that all of the films are free from cracks (note: some of the films showed some cracking at their edges and at the film–substrate interface). However, some of the films show minor imperfections that appear to be air bubbles trapped in the film during deposition. The most striking observation from the micrographs is the evidence for phase segregation in films containing both organosilanes and polymer additives (images d and f). These films show a highly variable distribution of "islands" and "channels" of different composition, perhaps reflecting polymer-rich or organosilane-rich regions within the

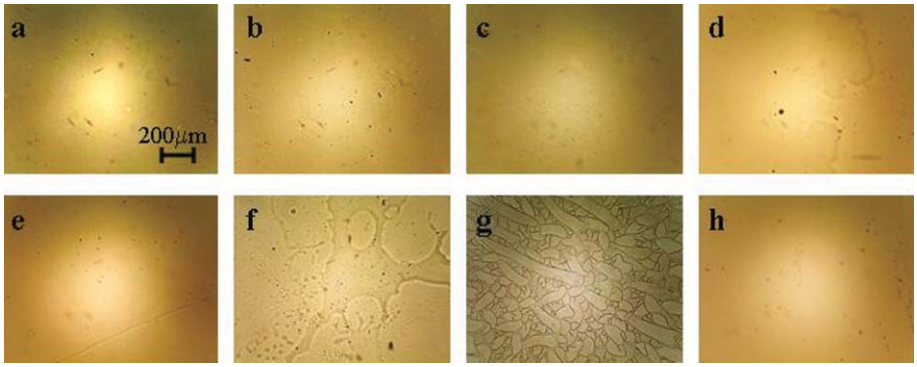

Fig. 2 Optical micrographs of thin films after casting (panels a–f) and after rehydration by immersion in water (panels g and h). (a) TEOS, (b) TEOS + 3% PEG, (c) 20% MTES, (d) 20% MTES + 3% PEG, (e) 10% DMDMS, (f) 10% DMDMS + 3% PEG, (g) rehydrated film of TEOS, (h) rehydrated film of 10% DMDMS + 3% PEG. All films were obtained at a withdrawal speed of 4mm min^{-1} and were aged for 3 days before imaging.

films. The morphology of the films observed by optical microscopy did not change as the samples were aged for up to 60 days, showing that the films do not undergo macroscopic structural rearrangements during long-term aging. It should be noted that even those films that appear to be homogeneous may still show phase segregation on a scale that is below the resolution of the optical microscope. We are currently examining the various thin films using other imaging methods, such as atomic force microscopy, transmission electron microscopy, and environmental scanning electron microscopy, to further assess phase segregation within such films. These results will be reported in an upcoming publication.

Addition of water to the films led to extensive cracking of many of the films [Fig. 2(g) is a representative image of a rehydrated TEOS-derived film, while Fig. 2(h) shows a rehydrated film containing 10% DMDMS]. The general trends observed from the optical micrographs were as follows: (1) TEOS films tended to crack more extensively than organosilane-loaded films, suggesting that the lower dipolarity of the organosilanes films prevented uptake of water and reduced hydration stress;[37] (2) films produced at faster withdrawal speeds (*i.e.* thicker films) showed more cracking than those produced at slower withdrawal speeds; (3) addition of PEG to TEOS-derived films improved the resistance of the films to cracking, likely owing to greater hydration of the films during drying, and, hence, a lower extent of hydration stress during rehydration; (4) aging of films led to improved resistance to cracking, with films showing poorer stability to cracking at early aging times (less than 10 days after casting), but improved durability as aging continued, with films over 60 days old showing no cracking. Hence, the highest quality films appear to be those formed from TEOS with PEG, or from DMDMS or MTES without PEG, as such films showed the least cracking and were the most microscopically homogenous in terms of composition.

Evolution of internal environment during film aging

PRODAN fluorescence. PRODAN provides information on the internal dipolarity of the solvent entrapped within sol–gel-derived materials, and also shows a characteristic emission band at *ca.* 440 nm, which is related to the formation of PRODAN aggregates when the probe exceeds its solubility limit.[34,38–43] Fig. 3 shows emission spectra obtained from PRODAN within TEOS-derived films over the first hour of aging. Immediately after casting (1 min) the spectrum shows a single emission band centered at *ca.* 475 nm, indicative of a film containing a significant level of ethanol. However, the spectrum of the entrapped probe rapidly evolves (over 8.5 min) such that the major emission band shifts to *ca.* 530 nm, with an additional minor emission band emerging at 440 nm, consistent with the presence of a small fraction of PRODAN aggregates. The emission spectrum of the casting solution, both before and after gelation, was centered at 475 nm and showed no emission band at 440 nm. Furthermore, none of the other film compositions resulted in the appearance of a PRODAN aggregate emission band at any time. These results suggest that (1) the rapid loss of ethanol from the TEOS-based film immediately upon casting, and the resultant decrease in PRODAN solubility, are likely responsible for the significant aggregate emission band[17] and (2) the presence of non-polar additives such as MTES, DMDMS, or PEG results in solubilization of PRODAN.[10]

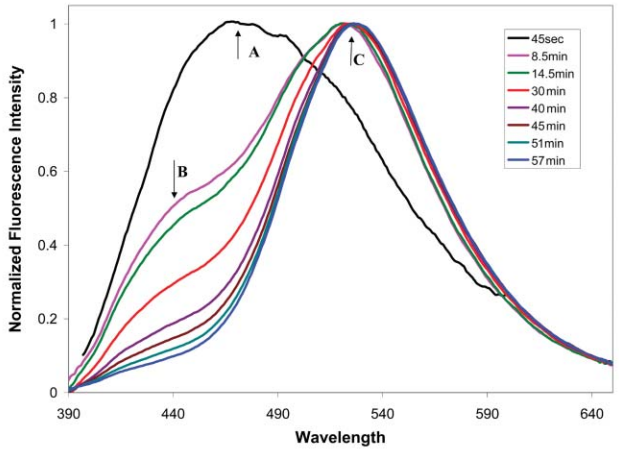

Fig. 3 Emission spectra of PRODAN obtained from a TEOS film over its first hour of aging. The acquisition times are listed on the figure. Arrow A shows the emission at 475 nm obtained 45 s after casting the TEOS thin film. Arrow B shows the emission peak at 440 nm, indicating the presence of the PRODAN aggregate emission maximum band, which decreases with time. Arrow C shows the emission at 525 nm, which corresponds to the final location of the PRODAN spectrum in pure TEOS thin films.

As aging continued, the emission band intensity at 440 nm decreased significantly, suggesting that the probe slowly associated with the silane surface and dissociated back to the monomeric form. This is in agreement with the observation that the PRODAN aggregate band in bulk TEOS glasses slowly decreases in intensity after many months of aging.[34] These results show that drying and aging of films are accelerated significantly relative to the same processes in bulk glasses.

Fig. 4 shows the evolution of the PRODAN emission maxima for each of the six films during the first 5 h of aging (panel A) and as aging continued for up to 80 days (panel B). All samples began with similar emission maxima of

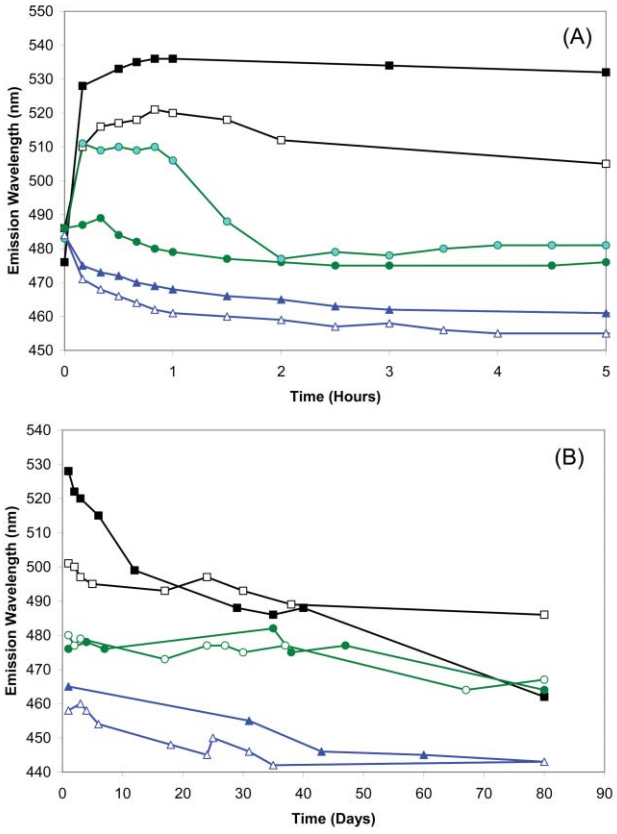

Fig. 4 Evolution of the PRODAN emission maxima for each of the six films from the point of casting onto the slide over the first 5 h (panel A) and over the remaining 80 days (panel B). TEOS (■), TEOS + 3% PEG (□), 20% MTES (●), 20% MTES + 3% PEG (○), 10% DMDMS (▲), 10% DMDMS + 3% PEG (△). Typical errors are ±2 nm.

475–485 nm (reflecting similar environments for the probe). Over the first 30 min, many of the films underwent rapid changes in emission wavelength, consisting of either a red shift in the emission wavelength, owing to the loss of ethanol (TEOS, TEOS/PEG, MTES/PEG), a blue shift in the emission maximum, owing to the loss of water from the interior of the film and/or adsorption of the probe onto the silica surface (DMDMS films with or without PEG), or no significant change (MTES). Between 1 and 2 h after casting, the polar films begin to show a significant blue shift, likely owing to the loss of entrapped water. The most significant shift occurs in films derived from MTES/PEG, which may reflect adsorption of the probe from the solvent phase onto methyl groups that are located on the pore wall and/or preferential partitioning of the probe into an MTES-rich phase as the water is lost. The film polarity begins to stabilize after 2 h, and shows only minor shifts in polarity over the next 3 months, signifying a slower change in the film properties that are consistent with the syneresis process.

The emission wavelength values 5 h after casting reflect the internal polarity of the various films, with polar films (TEOS) emitting at longer wavelengths and films containing either an organosilane or polymer emitting at shorter wavelengths, consistent with a more hydrophobic environment. It is interesting to note that while MTES- and DMDMS-doped films have a similar number of alkyl groups, the dipolarity of DMDMS films was substantially lower than for MTES, suggesting that the probe may have preferentially associated with DMDMS. In each case, the addition of PEG led to decreased polarity of the internal environment, with samples containing both an organosilane and PEG being the most non-polar ($\lambda_{em} \approx 460$ nm). The significant blue shift in the PRODAN emission spectra in the presence of PEG reflects decreases in hydrogen bonding between the probe and the solvent and/or silica surface.[44] Overall, these results show that it is possible to control the internal environment within the sol–gel-derived films over a wide range, and that both organosilane and polymer additives can be used for this purpose. This level of control over the internal environment is likely to be useful for optimizing the thin films to produce maximum fluorescence signaling capability[45] or optimal protein stability.[46]

As the films aged for a further 80 days, it became clear that the films continue to evolve, as demonstrated by the continual blue shift of up to 60 nm in the emission spectra for the different films. Such an evolution of the film dipolarity/chemistry has been noted before by Bright and co-workers,[28,47] who reported that the accessibility of entrapped pyrene to oxygen decreased over a period of 1 year. The final emission maximum of PRODAN in the aged films ranged from 490 (TEOS/PEG) to *ca.* 440 nm (10% DMDMS with or without PEG). These shifts are consistent with slow conversion of silanol groups to siloxanes, which would be expected to lower the overall dipolarity.[3] TEOS films containing PEG do not undergo as substantial a change in polarity as the other films, suggesting that the PEG may aid water retention within the polar TEOS films, thus slowing the change in film polarity (note: TEOS/PEG films eventually evolved to show emmission maxima at 460 nm over a period of 10 months). Overall, the fluorescence results suggest that the films age in two distinct stages; an initial rapid drying step, consistent with solvent loss, and a long-term evolution of the films, consistent with slower syneresis and aging of the glass. This is distinct from bulk glasses, where these two processes occur simultaneously.[10]

While the trend of a two-stage aging process for thin films, consisting of a rapid initial change in film composition followed by a slower aging process, has been previously reported in the literature,[10,34] no previous reports describe the aging of films formed by our two-step process in comparison to either identically formed bulk glasses or films formed with high levels of alcohol. In general, the aging of our films, while faster than comparable bulk glasses by approximately two orders of magnitude (hours *vs.* months), is slower than the aging of alcohol-rich films, which have been reported to undergo aging in as little as 15 s.[16] It should also be noted that the high alcohol content that was present in previously reported thin films is not likely to be amenable to the entrapment of biomolecules, and thus it is important to understand how biocompatible thin films age so as to optimize the stability of entrapped proteins, as described below.

Characteristics of entrapped HSA

Fig. 5(A) shows the background-corrected and normalized fluorescence emission spectra of native HSA in aqueous buffer (curve A), in 1 M GdHCl (curve B) and in 4 M GdHCl (curve C) as compared to the emission maximum of HSA entrapped in each of the thin films [Fig. 5(B)]. The emission spectra of the entrapped HSA samples are all blue shifted relative to the spectrum of native HSA in solution, and are very similar to the spectrum of HSA in 1 M GdHCl. Specific emission maximum values were as follows: native HSA = 337, 1 M GdHCl = 330, 4 M GdHCl = 345, TEOS = 331, TEOS/PEG = 331, 20% MTES = 331, 20% MTES/PEG = 331, 10% DMDMS = 332, 10% DMDMS/PEG = 327 nm.

The blue shift suggests that the HSA may adopt a somewhat extended conformation, which results in the sequestering of the Trp residue into a hydrophobic pocket of domain II.[48,49]

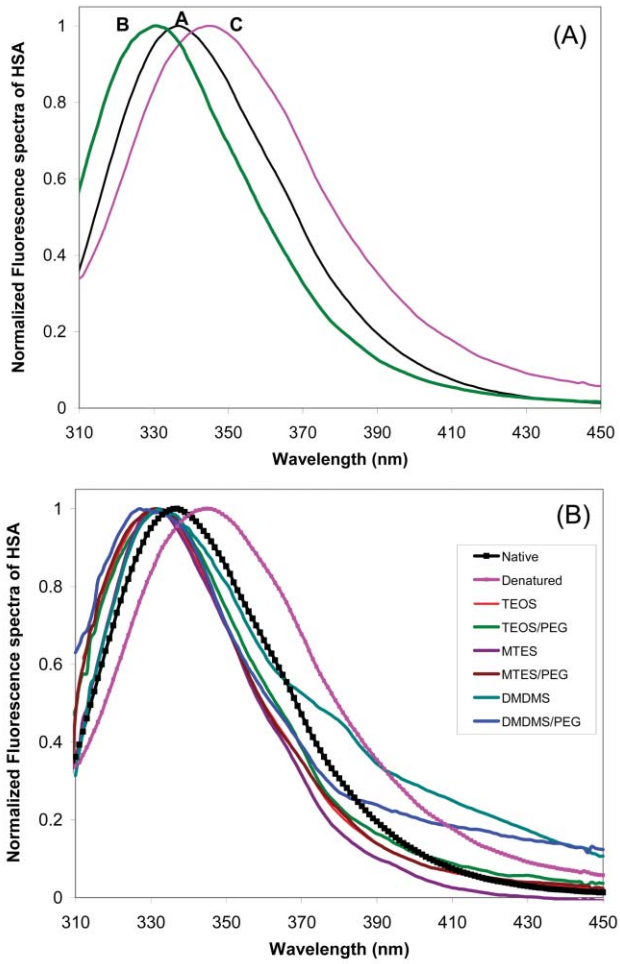

Fig. 5 Background-corrected and normalized fluorescence emission spectra obtained from HSA in solution (spectrum A), in 1 M GdHCl (spectrum B) and in 4 M GdHCl (spectrum C) (A) and for HSA entrapped in each of the thin films (B). Spectra A and C from panel A are also included to provide a basis for comparison of spectra for free and entrapped proteins.

However, previous reports show that the expanded form of HSA retains the ability to bind ligands, and thus this conformation does not necessarily reflect a denatured form of the protein. Loss of ligand binding ability generally occurs upon unfolding of domain II, which tends to correspond to a significant red shift in the emission maximum.[48]

As shown in Fig. 5, films prepared from either DMDMS or DMDMS/PEG showed significant emission intensity in the region between 380 and 440 nm, indicative of a fraction of HSA which is in an aggregated form. Such films also show a somewhat larger blue shift than does HSA in TEOS or MTES-derived films, suggesting that DMDMS may have directly interacted with the Trp residue of HSA. Overall, these results show that the inclusion of the MTES or polymer additives is compatible with the entrapment of HSA in a native conformation, while inclusion of the more hydrophobic DMDMS additive appears to cause the entrapped protein to undergo a significant conformational change that exposes the Trp residue to the hydrophobic additive.[12]

To determine if the observed changes in protein conformation were related to denaturation of the entrapped protein, the ability of the entrapped protein to bind to the ligand salicylate was examined. These results were compared to those obtained for native and denatured HSA in solution, as shown in Fig. 6. A decrease in Trp emission intensity was observed in all films, including those derived from DMDMS, suggesting that in all cases the entrapped protein bound to salicylate, and thus retained at least partial function compared to HSA in solution. This shows that the entrapment method did not irreversibly alter the functional form of the protein. All of the curves are consistent with saturation binding, and all show saturation in the micromolar binding region.

The binding curves reveal several points that merit special attention. First, all of the entrapped protein samples appear to show higher binding to salicylate than is observed in solution. This is not likely to be due to an increase in the binding constant of the entrapped protein. Rather, it is more likely to be due to enhanced partitioning of salicylate from solution into the film *via* a solid-phase microextraction process[12] and/or subtle differences in the photophysics of tryptophan within each of the films, which may have led to enhanced quenching by salicylate. Second, films containing PEG appear to show a larger fluorescence response than do films without PEG; however, this again reflects enhanced quenching of the Trp residue in the presence of PEG, which was noted to decrease the intensity of Trp fluorescence from HSA in solution. Third, the film derived from DMDMS/PEG shows an unusually shaped binding curve and extremely high levels of quenching of Trp, which may reveal that HSA is in such films is denatured, thus exposing the Trp residue and leading to direct interactions between the Trp residue and salicylate.

Overall, the results clearly show that it is possible to prepare high quality films and to entrap functional HSA within such films using the 2-step sol–gel processing method involving sonication of precursors followed by addition of a buffered solution containing the protein. This is in agreement with recent results from our research group, which show that such films are capable of maintaining the activity of entrapped lipase for detection of glyceryl tributyrate.[45] The PRODAN results offer insight into the rapid drying and slow aging processes that occur within these thin films. The consecutive nature of the drying and aging processes in thin films is very different from that of monolithic blocks, where these two processes occur simultaneously. The rapid evolution of these films suggests that it should be possible to use the films only hours after formation. Unfortunately, the slow aging process observed for the films, which continues over periods of months, may lead to difficulties with long-term drift in the calibration of analytical instruments. Further studies on the application of such films to biosensor platforms based on optical fibers and planar waveguides are underway and will be reported in due course.

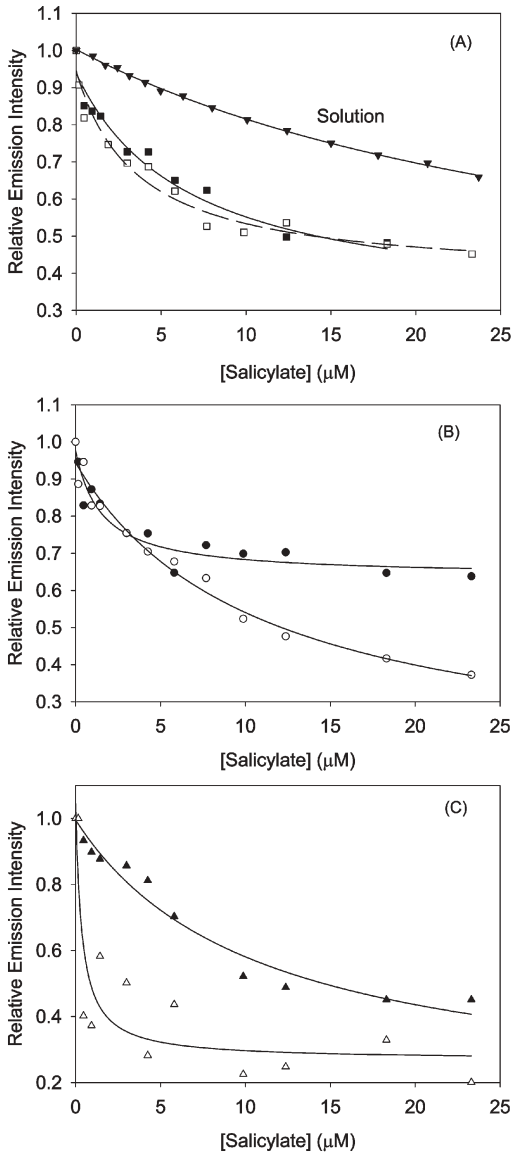

Fig. 6 Salicylate binding to the human serum albumin in solution and when entrapped into sol–gel-derived thin films: (A) Solution (▼), TEOS (■), TEOS + 3% PEG (□); (B) 20% MTES (●), 20% MTES + 3% PEG (○); 10% DMDMS (▲), 10% DMDMS + 3% PEG (△). Typical errors for solution and TEOS- and MTES-derived thin films are ±0.03; for DMDMS-derived thin films the errors are ±0.10.

Acknowledgements

We would like to thank the Natural Sciences and Engineering Research Council of Canada for financial support of this work. We would also like to acknowledge Michael Rakic and Adam Bryant for technical assistance, and Professor Harald Stöver and Professor Adrian Kitai for providing access to optical microscopy and profilometry equipment. J. D. B. holds the Canada Research Chair in Bioanalytical Chemistry at McMaster University.

References

1 S. Braun, S. Rappoport, R. Zusman, D. Avnir and M. Ottolenghi, *Mater. Lett.*, 1990, **10**, 1.
2 L. L. Hench and J. K. West, *Chem. Rev.*, 1990, **90**, 33.
3 C. J. Brinker and G. W. Scherer, *Sol-Gel Science: The Physics and*

Chemistry of Sol-Gel Processing, Academic Press, San Diego, 1991.
4 A. Turniansky, D. Avnir, A. Bronshtein, N. Aharonson and M. Altstein, *J. Sol-Gel Sci. Technol.*, 1996, **7**, 135.
5 U. Narang, P. N. Prasad, F. V. Bright, A. Kumur, N. D. Kumur, B. D. Malhotra, M. N. Kamalasanan and S. Chandra, *Chem. Mater.*, 1994, **6**, 1596.
6 R. A. Caruso and M. Antonietti, *Chem. Mater.*, 2001, **13**, 3272.
7 G. A. Baker, S. Pandey, E. P. Maziarz III and F. V. Bright, *J. Sol-Gel Sci. Technol.*, 1999, **15**, 37.
8 G. A. Baker, J. D. Jordan and F. V. Bright, *J. Sol-Gel Sci. Technol.*, 1998, **11**, 43.
9 P. Lesot, S. Chapuis, J. P. Bayle, J. Rault, E. Lafontaine, A. Campero and P. Judeinstein, *J. Mater. Chem.*, 1998, **8**, 147.
10 T. Keeling-Tucker, M. Rakic, C. Spong and J. D. Brennan, *Chem. Mater.*, 2000, **12**, 3695.
11 M. T. Reetz, A. Zonta and J. Simpelkamp, *Biotechnol. Bioeng.*, 1996, **49**, 527.
12 J. D. Brennan, J. S. Hartman, E. I. Ilnicki and M. Rakic, *Chem. Mater.*, 1999, **11**, 1853.
13 N. Wittouck, F. De Schryver and I. Snijkers-Hendrickx, *J. Sol-Gel Sci. Technol.*, 1997, **8**, 895.
14 D. Avnir, S. Braun, O. Lev and M. Ottolenghi, *Chem. Mater.*, 1994, **6**, 1605.
15 M. Guglielmi, P. Colombo, F. Peron and L. M. D. Esposti, *J. Mater. Sci.*, 1992, **27**, 5052.
16 F. Nishida, J. M. McKiernan, B. Dunn, J. I. Zink, J. C. Brinker and A. J. Hurd, *J. Am. Ceram. Soc.*, 1995, **78**, 1640.
17 M. H. Huang, H. Soyez, B. S. Dunn and J. I. Zink, *Chem. Mater.*, 2000, **12**, 231.
18 K. Flora and J. D. Brennan, *Analyst*, 1999, **124**, 1455.
19 T. M. Butler, B. D. MacCraith and C. McDonagh, *J. Non-Cryst. Solids*, 1998, **224**, 249.
20 G. C. Righini and S. J. Pelli, *J. Sol-Gel Sci. Technol.*, 1997, **8**, 1991.
21 D. D. Dunawila, B. A. Torgerson, C. K. Chang and K. A. Berglund, *Anal. Chem.*, 1994, **66**, 2739.
22 U. Narang, P. N. Prasad, F. V. Bright, K. Ramanathan, N. D. Kumar, B. D. Malhotra, M. N. Kamalasanan and S. Chandra, *Anal. Chem.*, 1994, **66**, 3139.
23 B. C. Dave, H. Soyez, J. M. Miller, B. Dunn, J. S. Valentine and J. I. Zink, *Chem. Mater.*, 1995, **7**, 1431.
24 B. C. Dave, J. M. Miller, B. Dunn, J. S. Valentine and J. I. Zink, *J. Sol-Gel Sci. Technol.*, 1997, **8**, 629.
25 J. D. Jordan, R. A. Dunbar and F. V. Bright, *Anal. Chim. Acta*, 1996, **332**, 83.
26 K. R. Rogers and E. J. Poziomek, *Chemosphere*, 1996, **33**, 1151.
27 A.-C. Chang, J. B. Gillespie and M. B. Tabacco, *Anal. Chem.*, 2001, **73**, 467.
28 R. A. Dunbar, J. D. Jordan and F. V. Bright, *Anal. Chem.*, 1996, **68**, 604.
29 N. Uchida, N. Ishiyama, Z. Kato and K. Uematsu, *J. Mater. Sci.*, 1994, **29**, 5188.
30 A. Panusa, A. Flamini and N. Poli, *Chem. Mater.*, 1996, **8**, 1202.
31 R. Wang, U. Narang, P. N. Prasad and F. V. Bright, *Anal. Chem.*, 1993, **65**, 2671.
32 J. S. Lundgren and F. V. Bright, *Anal. Chem.*, 1996, **68**, 3377.
33 G. Weber and F. J. Farris, *Biochemistry*, 1979, **18**, 3075.
34 K. K. Flora and J. D. Brennan, *J. Phys. Chem. B.*, 2001, **105**, 12003.
35 L. Zheng, W. R. Reid and J. D. Brennan, *Anal. Chem.*, 1997, **69**, 3940.
36 E. Matijevic, *Acc. Chem. Res.*, 1981, **14**, 22.
37 J. Zarzycki, M. Prassas and J. Phalippou, *J. Mater. Sci.*, 1982, **17**, 3371.
38 A. Balter, W. Nowak, W. Pawelkiewicz and A. Kowalcyzk, *Chem. Phys. Lett.*, 1988, **143**, 565.
39 C. F. Chapman and M. Maroncelli, *J. Phys. Chem.*, 1990, **94**, 4929.
40 C. F. Chapman and M. Maroncelli, *J. Phys. Chem.*, 1991, **95**, 9095.
41 J. Zeng and P. L. Chong, *Biochemistry*, 1991, **30**, 9485.
42 C. E. Bunker, T. L. Bowen and Y.-P. Sun, *Photochem. Photobiol.*, 1993, **58**, 499.
43 S. Sun, M. P. Heitz, S. A. Perez, L. A. Colon, S. Bruckenstein and F. V. Bright, *Appl. Spectrosc.*, 1997, **51**, 1316.
44 U. Narang, J. D. Jordan, F. V. Bright and P. N. Prasad, *J. Phys. Chem.*, 1994, **98**, 8101.
45 M. D. Gulcev, G. Goring, M. Rakic and J. D. Brennan, *Anal. Chim. Acta*, 2002, **457**, 47.
46 W. Jin and J. D. Brennan, *Anal. Chim. Acta*, 2002, **461**, 1.
47 N. J. Bonzagni, G. A. Baker, S. Pandey, E. D. Niemeyer and F. V. Bright, *J. Sol-Gel Sci. Technol.*, 2000, **17**, 83.
48 K. K. Flora, J. D. Brennan, G. A. Baker, M. A. Doody and F. V. Bright, *Biophys. J.*, 1998, **75**, 1084.
49 K. K. Flora and J. D. Brennan, *Chem. Mater.*, 2001, **13**, 4170.